Analytical Biochemistry 609 (2020) 113908

Contents lists available at ScienceDirect

Analytical Biochemistry

journal homepage: www.elsevier.com/locate/yabio

Electrochemical biosensor for miRNA-21 based on gold-platinum bimetallic nanoparticles coated 3-aminopropyltriethoxy silane

Anu Bharti [a], Sakshi Mittal [a], Shilpa Rana [a], Divya Dahiya [b], Navneet Agnihotri [a,**], Nirmal Prabhakar [a,*]

[a] Department of Biochemistry, Panjab University, Chandigarh, India
[b] Department of Surgery, PGIMER, Chandigarh, India

ARTICLE INFO

Keywords:
MicroRNA-21
Electrochemical biosensor
3-Aminopropyltriethoxy silane
Bimetallic nanoparticles
Hybridization assay
Aminylated cDNA

ABSTRACT

We report an electrochemical biosensor based on gold platinum bimetallic nanoparticles (AuPtBNPs)/3-aminopropyltriethoxy silane (APTS) nanocomposite coated fluorine-doped tin oxide (FTO) as a biosensing platform for hybridization-based detection of miRNA-21. Field Emission-Scanning Electron Microscopy (FE-SEM), Fourier Transform Infrared Spectroscopy (FT-IR) and electrochemical measurements were carried out to ensure the successful construction of the biosensor. The amount of cDNA immobilized on electrode surface and hybridization time required for the miRNA-21 sensing were optimized. The biosensing platform showed detection limit of 0.63 fM with wide linear range i.e. 1 fM-100 nM for miRNA-21 detection. The biosensing strategy demonstrates a good recovery yield from 90.18% to 94.6% in serum samples. It offers good selectivity for its complementary miRNA compared to the non-complementary miRNAs. Other analytical features of the biosensor such as stability, reusability and reproducibility were also tested, providing appropriate results.

1. Introduction

MicroRNAs (miRNAs) are small non-coding RNA sequences (20–22 nucleotide in length) that post transcriptionally regulate the gene expression of target mRNAs. They also regulate many biological processes like cell proliferation, differentiation, aging, cellular apoptosis and tumorigenesis [1–3]. It was found that there are more than 2500 miRNA sequences in the human genome, regulating about 30% of the protein coding genes [4,5]. Abnormally expressed miRNAs leads to the development of cancer via various mechanisms including amplification, silencing, deletion and mutations [6]. They are present in the peripheral circulation and can be used as potential biomarkers for disease diagnosis, prognosis and therapy monitoring. MiRNAs are highly involved in the development of various types of cancers like colon cancer [7], prostate cancer [8], breast cancer [9], lung cancer [10] and ovarian cancer [11], and are differentially expressed in the blood circulations of affected as well as healthy individuals.

Over the past few years, the incidences of breast cancer are increasing devastatingly and have become a serious threat to the women health throughout the world [12]. Early stage detection of breast cancer could enable appropriate treatment method for frequent recovery and also avoid unnecessary surgeries. Studies have found that miRNA-21 is one of the most frequently upregulated microRNA in breast carcinomas [13–16]. Its overexpression is highly correlated with the specific pathological features of breast cancer like metastasis, tumor stage and survival of the patients etc. [17]. Conventional techniques used for miRNA detection such as northern blotting [18], microarray [19] and real time-PCR [20] are associated with some disadvantages like very high operational cost, time consuming, complex instrumentation and procedures [21]. To avoid these complications, biosensors are available with numerous advantages such as cost effectiveness, less invasive, more sensitive and provide point-of-care (POC) diagnosis. Many biosensing strategies have been introduced by the researchers for miRNA detection such as photoluminescence [22], surface plasmon resonance [23], colorimetric [24], field-effect transistor devices [25] and most commonly electrochemical approaches [26].

The electrochemical biosensors having nanomaterial as immobilization platforms are drawing much attention in the diagnostic field due to its high sensitivity and selectivity, miniaturization, low cost, easy operation, portability and quick response [27–29]. Numerous signal

* Corresponding author.
** Corresponding author.
E-mail addresses: agnihotri.navneet@gmail.com (N. Agnihotri), nirmalprabhakar@gmail.com (N. Prabhakar).

https://doi.org/10.1016/j.ab.2020.113908
Received 13 May 2020; Received in revised form 4 August 2020; Accepted 7 August 2020
Available online 18 August 2020
0003-2697/

amplification approaches based on duplex specific nuclease (DSN) [30], DNA strand displacement reaction (SDR) [31], electrochemical-chemical-chemical (ECC) redox cycling [32], rolling circle amplification [33], microfluidic paper based analytical devices (μPADs) [34] and hybridization chain reaction [35] etc. are being explored for miRNA-21 detection. Wang and co-workers established an enzymatic and molecular beacon mediated strand displacement amplification methodology for electrochemical sensing of miRNA-21 [36]. The developed strategy showed detection limit of 40 pM for miRNA-21 at optimized conditions. Shuai et al., fabricated a sandwich-type electrochemical assay using MgO nanoflower/AuNPs as sensing platform and GO–AuNPs hybrids as carriers in combination with ECC redox cycling detection system [37]. The biosensor exhibited a detection limit of 50 aM for the detection of miRNA-21. Liu and his research group proposed a detection method for miRNA-21 using Fe_3O_4/CeO_2 @Au MNPs nanocatalyst and catalytic hairpin assembly (CHA) for signal amplification which provided detection limit of 0.33 fM within a linear range of 1 fM to 1 nM [38]. Recently, a triple signal amplification strategy was developed by combining DSN assisted target recycling with gold nanoparticles and horseradish peroxidase (HRP) enzyme signal amplification [39]. DSN works by cleaving the double stranded DNAs and DNA/RNA hybrids whereas it is inactive to single or double stranded RNAs. So, the target miRNA hybridizes with the hairpin DNA to form a duplex (DNA/RNA) and can be easily cleaved by DSN resulting in the release of miRNA for further hybridization event to occur.

The hybridization based detection method is considered as a simple and effective strategy for biosensor development. We have recently fabricated a hybridization based electrochemical biosensor for miRNA-21 detection using gold-platinum bimetallic nanoparticles (AuPtBNPs) decorated carboxylated graphene oxide sheets as signal amplification strategy and biotin labelled capture probe sequence as recognition element [40]. The developed biosensor has shown good results with detection limit 1 fM for miRNA-21. Hence, the current work has been extended for improved and better diagnosis of breast cancer biomarker. Focus has been drawn towards the detection of miRNA-21, combining the properties of 3-aminopropyltriethoxy silane (APTS) and AuPtBNPs. In the previous method, we have used biotinylated cDNA probe whereas aminylated cDNA (Am-cDNA) probe is used in this work for hybridization based detection of miRNA-21. For the immobilization of cDNA probe to the electrode surface, glutaraldehyde (GA) is used as a linker in spite of streptavidin. Thus, the presented biosensing platform exhibit greater physical strength than the previous one due to the adhesive nature of glutaraldehyde which protects the fabricated material from getting off the electrode surface. Also, the use of high cost molecules like streptavidin and biotin in the previous work makes the method costly compared to the present strategy. Bimetallic nanoparticles are in frequent use now days because of their excellent electronic properties, better catalytic activity and resistance to deactivation [41–43]. The conductive nature of gold nanoparticles could greatly enhance the sensitivity of biosensing method in combination with platinum nanoparticles. Both the metal nanoparticles show synergistic effect in combination with each other to improve their properties instead of applying individually for biosensor development [44]. Electrochemical method of synthesis is preferred choice for uniform deposition of bimetallic nanoparticles on electrode surface [45]. Furthermore, APTS is a silica derivative and useful for the functionalization of various biosensing platforms with free amino groups forming an active monolayered surface [46,47]. The silane groups present on APTS gets firmly attached to the silicon or glass substrates through hydroxyl groups exposed on its surface. FTO has been used in this study which is a conducting fluorine-doped tin oxide transparent glass and can be used as a base electrode in various electrochemical biosensing applications. FTO offers many advantages including fast electron transfer, large surface area, mechanical strength and chemical as well as temperature stability.

2. Experimental

2.1. Materials and reagents

Fluorine-doped tin oxide (FTO) sheets, (3-Aminopropyl) triethoxysilane, ammonium hydroxide (NH_4OH), hydrogen peroxide (H_2O_2), chloroplatinic acid (H_2PtCl_6) and chloroauric acid ($HAuCl_4$) were purchased from Sigma-Aldrich, USA. Sodium sulfate (Na_2SO_4) was received from SDFCL, Mumbai, India. Glutaraldehyde ($C_5H_8O_2$), potassium ferrocyanide trihydrate ($K_4Fe(CN)_6{\cdot}3H_2O$), potassium ferricyanide ($K_3Fe(CN)_6$), tris hydroxymethyl aminomethane (Tris), ethylene diamine tetra acetic acid (EDTA) and sodium chloride (NaCl) were supplied by HiMedia Laboratory Pvt. Ltd., Mumbai, India. All the reagents were of analytical grade. The base sequences used in this study were synthesized by Sigma-Aldrich, USA. These sequences were taken from our previous work [40] given in supplementary section Table S1.

Autoclaved glasswares and deionized water (dH_2O) was used to prepare all the solutions throughout the study. The base sequences were dissolved in TE buffer (tris 10 mM, pH 7.5 + EDTA 1 mM, pH 8.0) and stored at −20 °C. The electrochemical measurements were carried out in $[Fe(CN)_6]^{3-/4-}$ electrolyte solution and prepared by dissolving 5 mM of potassium ferricyanide and 5 mM of potassium ferrocyanide trihydrate in phosphate buffer containing 0.9% NaCl.

2.2. Instruments

The morphological characterization of fabricated electrodes was done by FE-SEM [Hitachi SU8000]. Nicolet 1S50 was used for FT-IR analysis to check the functional groups present on FTO electrode after each modification step. Electrochemical studies were carried out on an AutoLab 302NFRA32 M [Metrohm-Autolab Instruments, Netherlands] workstation with a conventional three electrode system, an Ag/AgCl as reference electrode, a platinum wire as counter electrode and FTO as working electrode. Real time-PCR studies were done on CFX Real-Time PCR System [Bio-Rad].

2.3. Step wise modification of prepared biosensor

The prewashed FTO electrodes were dipped in a solution containing H_2O_2:NH_4OH:H_2O (1:1:5) for 30 min at 60 °C for hydroxylation process. The hydroxylated FTO electrodes were incubated in 2% APTS solution prepared in acetone for 24 h at room temperature. For deposition of AuPtBNPs, the dried APTS/FTO electrodes were immersed in a 0.2 M Na_2SO_4 solution containing 1.0 mM $HAuCl_4$ and 1.0 mM H_2PtCl_6 and subjected to a constant potential of −0.2 V for 350 s. The AuPtBNPs/APTS/FTO electrodes were rinsed with dH_2O and dried at room temperature for further use.

For the attachment of Am-cDNA on electrode surface, glutaraldehyde was introduced as a linker between exposed amine groups of silane moieties and Am-cDNA through its –CHO groups. The AuPtBNPs/APTS/FTO electrode was incubated with 1% glutaraldehyde solution for 2 h. Subsequently, 10 μL (20 μM) of Am-cDNA probe solution prepared in TE buffer was applied on the surface of GA/AuPtBNPs/APTS/FTO electrode. The modified electrode was rinsed with dH_2O to remove non-bound cDNA probe and stored at 4 °C for further use.

2.4. Electrochemical detection of miRNA-21

After the successful fabrication ofAm-cDNA/GA/AuPtBNPs/APTS/FTO bioelectrode, different concentrations of miRNA-21 ranging from 1 fM to 100 nM were tested by incubating for 20 min. The cDNA hybridized to its target miRNA-21 with strong affinity and produced concentration dependent signals which were measured electrochemically by DPV assay.

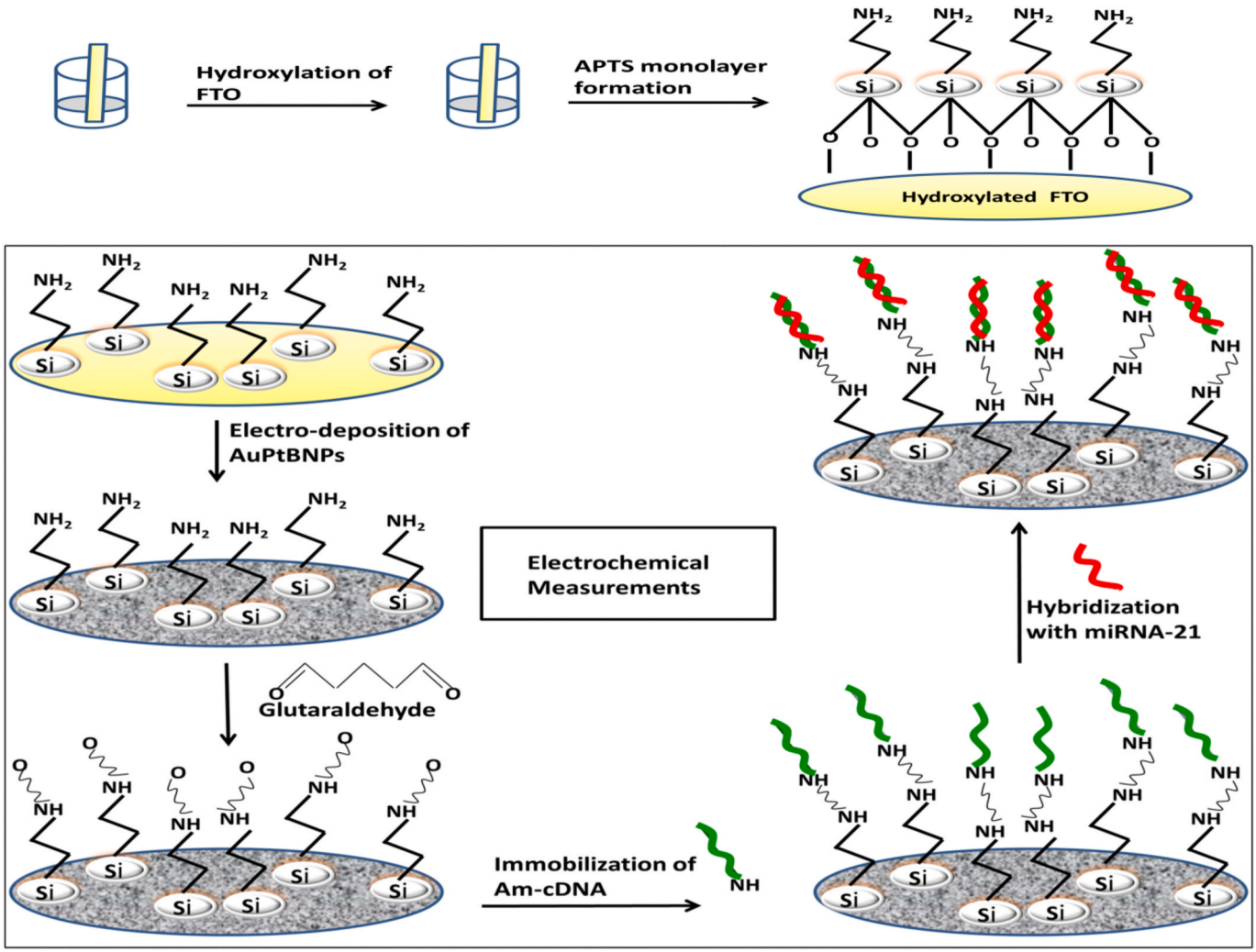

Fig. 1. Schematic illustration for the design and development of miRNA-21 biosensor.

2.5. Real sample analysis

The vulnerability of developed method in real samples was tested using serum samples of patients as well as healthy donors. Blood samples of breast cancer patients were collected from PGIMER, Chandigarh with ethical clearance (PGI/IEC/2016/3405). Five healthy and five diseased serum samples were diluted to 10 folds and subjected to the electrochemical detection of miRNA-21. Furthermore, recovery studies were also performed by spike-in different concentrations of standard miRNA-21 solution in diluted serum sample i.e. 1 pM, 1×10^2 pM, 1×10^3 pM and 1×10^4 pM. All these samples were applied on prepared electrode surface for 20 min and subjected for electrochemical measurements after washing.

2.6. Real time-PCR analysis of serum samples

The miRNA from serum samples was extracted using miRNeasy Mini kit (Catalogue # 217004, Qiagen, USA). The cDNA of extracted miRNA samples was generated by miRNA 1st strand cDNA synthesis kit (Cat #600036, Agilent Technologies, USA) following manufacturer's instructions and stored at −20 °C for further use. For real time-PCR analysis, 10 μL reaction mixture was prepared using following contents: 5 μL of SYBR Green master mix, 1.92 μL of forward/reverse primer mix, 1 μL of cDNA template and make up volume 10 μL with RNase free water. Finally, real time-PCR was conducted at 95 °C for 2 min, followed by 40 cycles of 95 °C for 5 s/60 °C for 15 s/72 °C for 20 s.

3. Results and discussion

3.1. Design principle of the developed biosensor

The stepwise modifications done on FTO electrode surface is demonstrated in Fig. 1. Firstly, the FTO electrodes were hydroxylated to introduce –OH moieties on electrode surface which aids in successful deposition of APTS monolayer through its silane moieties. After the formation of APTS/FTO electrode, AuPtBNPs were uniformly electrodeposited by applying −0.2 V potential for 350 s using chronoamperometry technique. The $–NH_2$ groups of APTS exposed on the other side provides the binding sites for biomolecule deposition and bimetallic nanoparticles greatly enhanced the electrochemical response of developed biosensor. Further, glutaraldehyde was introduced on the surface of AuPtBNPs/APTS/FTO as a linker between APTS and amine modified cDNA probe. Now, the cDNA probe coated electrode (Am-cDNA/GA/AuPtBNPs/APTS/FTO) is ready for target recognition on the basis of principle of hybridization.

3.2. Characterization of stepwise fabrication

3.2.1. FE-SEM

The morphological appearance of APTS, AuPtBNPs/APTS, GA/AuPtBNPs/APTS and Am-cDNA/GA/AuPtBNPs/APTS coated FTO were observed by FE-SEM imaging as shown in Fig. 2A. It can be seen in Fig. 2A(i) that APTS can form a thin layer over the surface of FTO

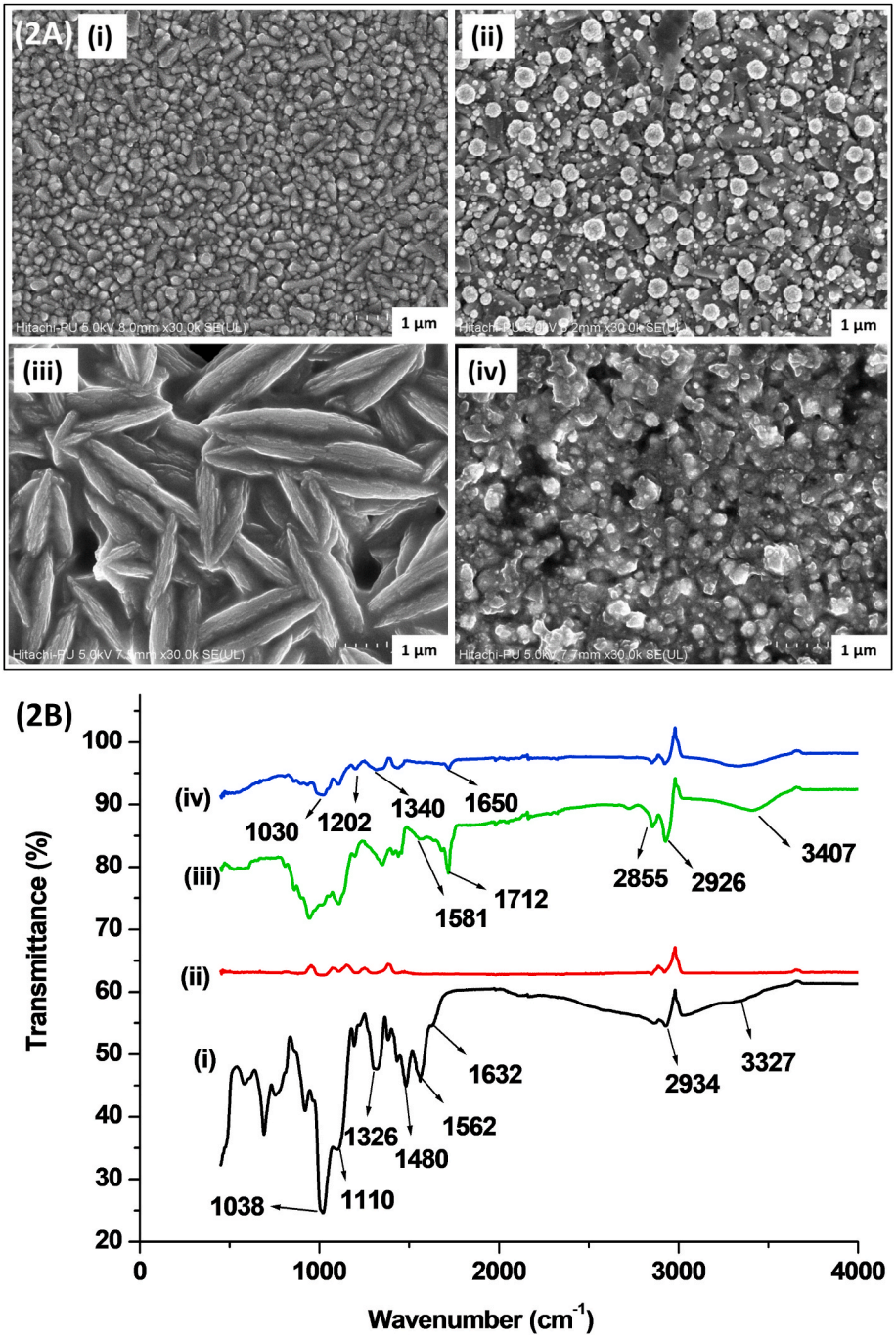

Fig. 2. (A) FE-SEM images & **(B)** FT-IR spectra of (i) APTS, (ii) AuPtBNPs/APTS, (iii) GA/AuPtBNPs/APTS and (iv) Am-cDNA/GA/AuPtBNPs/APTS coated FTO.

electrode. The electrodeposited AuPtBNPs on the surface of APTS/FTO shows uniform distribution of small round shaped flower like structures improving the electron transfer rate (Fig. 2A(ii)). After glutaraldehyde immobilization (Fig. 2A(iii)), a crystalline surface was observed which assisted the immobilization of cDNA probe on the electrode surface. Further modification with cDNA probe, structures having aggregated appearance were found aiding in the target hybridization (Fig. 2A(iv)). Hence, the change in morphological appearance after each step clearly indicated the successful deposition of all the materials and biomolecules.

3.2.2. FT-IR

Fig. 2B shows the FT-IR spectra of as prepared electrodes (i) APTS/FTO, (ii) AuPtBNPs/APTS/FTO, (iii) GA/AuPtBNPs/APTS/FTO and (iv) Am-cDNA/GA/AuPtBNPs/APTS/FTO. As shown in curve i, APTS displays peaks at 3327 cm^{-1}, 2934 cm^{-1}, 1632 cm^{-1}, 1562 cm^{-1}, 1480 cm^{-1}, 1326 cm^{-1}, 1110 cm^{-1} and 1038 cm^{-1} [48,49]. The peak at 3327 cm^{-1} is attributed to the presence of N–H stretch whereas peak related to N–H bending was found at 1632 cm^{-1}. The peaks at 2934 cm^{-1} and 1480 cm^{-1} correspond to N–CH_2 stretching. Other peak related to N–H bending was found at 1632 cm^{-1} and the peaks at 1562 cm^{-1} and 1326 cm^{-1} contributed to the presence of C–N stretch. The sharp peaks at 1110 cm^{-1} and 1038 cm^{-1} attributed to the stretching vibrations of Si–O–Si bond. All the observations affirmed the deposition of APTS on FTO electrode surface. In the spectrum of AuPtBNPs/APTS/FTO, there were no significant peaks for electrodeposited AuPtBNPs. After applying glutaraldehyde (curve iii), the appearance of absorption peak at 3407 cm^{-1} can be attributed to the O–H stretching vibrations. The peaks located at 2926 cm^{-1} and 2855 cm^{-1} can be assigned to C–H stretching

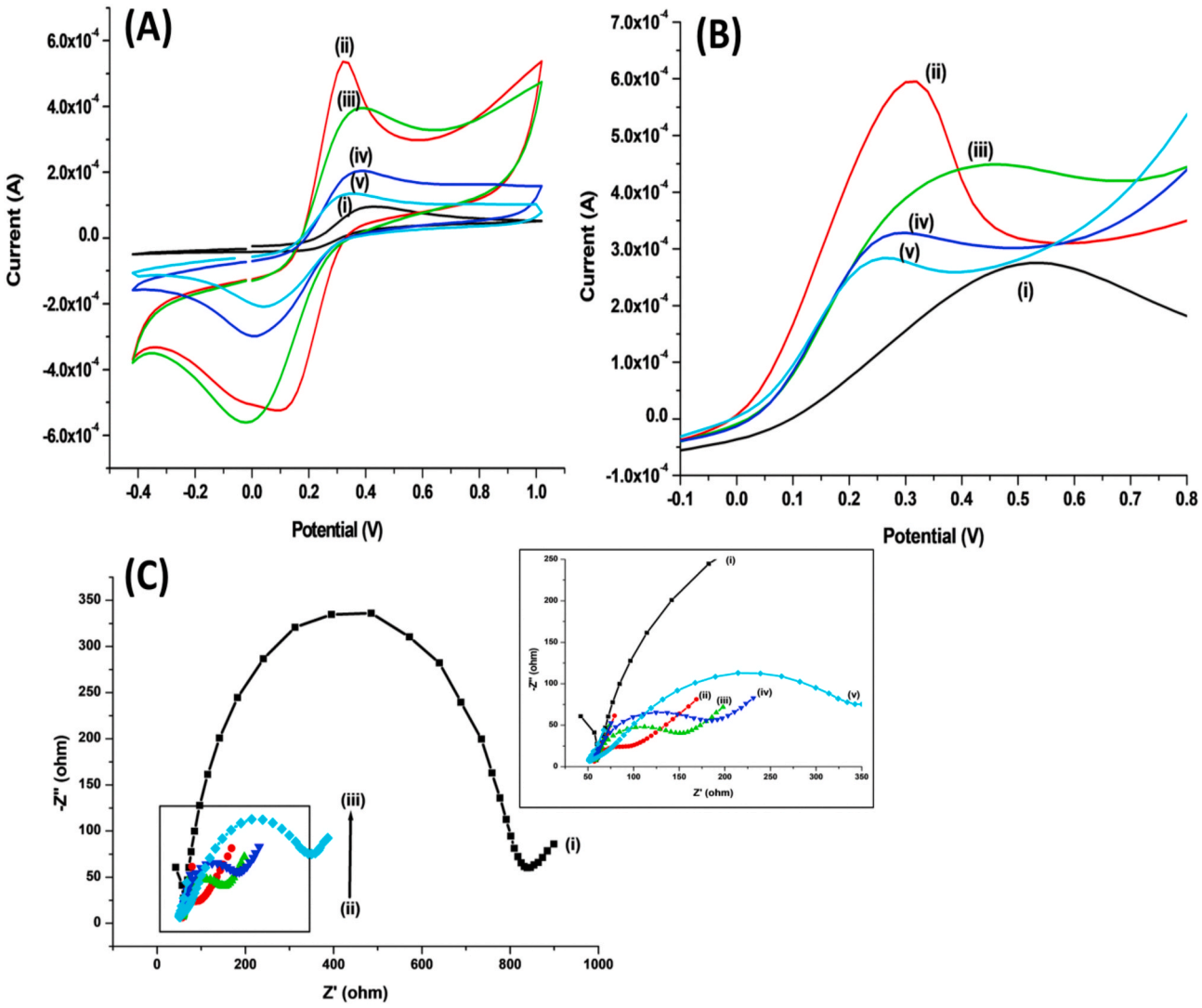

Fig. 3. (A) Cyclic voltammetry, **(B)** Differential pulse voltammetry and **(C)** Electrochemical impedance spectroscopy responses of (i) APTS, (ii) AuPtBNPs/APTS, (iii) GA/AuPtBNPs/APTS, (iv) Am-cDNA/GA/AuPtBNPs/APTS and (v) miRNA-21/Am-cDNA/GA/AuPtBNPs/APTS coated FTO (Inset: Stretched EIS results), in 50 mM PBS (pH-7.0, 0.9% NaCl) containing 5 mM $[Fe(CN)_6]^{3-/4-}$.

of aldehydes whereas the peaks at 1712 cm^{-1} and 1581 cm^{-1} are due to the presence of carbonyl group (C═O) [50,51]. In curve iv, the Am-cDNA/GA/AuPtBNPs/APTS/FTO electrode exhibited peaks at 1650 cm^{-1}, 1340 cm^{-1}, 1202 cm^{-1} and 1030 cm^{-1} [52]. The peaks at 1650 cm^{-1} and 1202 cm^{-1} can be assigned to the in-plane ring vibrations of thymine and sugar phosphate backbone present in ssDNA, respectively. The presence of C═C and C═N stretch of the pyrimidine and purine bases can be confirmed by peaks at 1340 cm^{-1} and 1030 cm^{-1}.

3.3. Electrochemical characterization of the biosensor

3.3.1. Cyclic voltammetry and differential pulse voltammetry

To analyze the electrochemical nature of fabricated materials, CV and DPV measurements were performed in 50 mM PBS (pH-7.0, 0.9% NaCl) containing 5 mM $[Fe(CN)_6]^{3-/4-}$. The cyclic voltammetry curves of APTS/FTO, AuPtBNPs/APTS/FTO, GA/AuPtBNPs/APTS/FTO, Am-cDNA/GA/AuPtBNPs/APTS/FTO and miRNA-21 coated Am-cDNA/GA/AuPtBNPs/APTS/FTO are shown in Fig. 3A. APTS coated FTO electrode showed very less peak current (9.39×10^{-5} A) (peak i), reflecting hindrance in the electron transfer between electrolyte solution and electrode surface. A significant increase in the peak current (5.37×10^{-4} A) (ii) was observed after coating AuPtBNPs on APTS/FTO due to highly conductive nature of bimetallic nanoparticles. When glutaraldehyde was applied, peak current decreased to 3.90×10^{-4} A (iii) because the negative charge present on its surface does not allow electron transfer from negatively charged electrolyte solution. Immobilization of Am-cDNA probe further decreased the peak current (2.01×10^{-4} A) (iv) attributing to the negatively charged phosphate backbone. After hybridization with miRNA-21, some more decrease in the peak current (1.31×10^{-4} A) (v) was seen due to the added hindrance effect of negatively charged phosphate backbones of both the single stranded probes. The DPV responses of corresponding fabricated electrodes are depicted in Fig. 3B. As observed in DPV results, the peak current showed very much similar trend to that of CV results. The results suggested successful fabrication of all the steps involved in the development of biosensor, as both the results are in good agreement with each other.

Furthermore, all the fabrication steps were also characterized electrochemically by EIS (Electrochemical Impedance Spectroscopy) method which measures the resistivity in the electron flow between electrolyte solution and electrode surface. Fig. 3C shows the EIS measurements of APTS/FTO, AuPtBNPs/APTS/FTO, GA/AuPtBNPs/APTS/FTO, Am-cDNA/GA/AuPtBNPs/APTS/FTO and miRNA-21 coated Am-cDNA/GA/AuPtBNPs/APTS/FTO taken in 50 mM PBS (pH-7.0, 0.9% NaCl) containing 5 mM $[Fe(CN)_6]^{3-/4-}$, at the frequency range from 0.1-

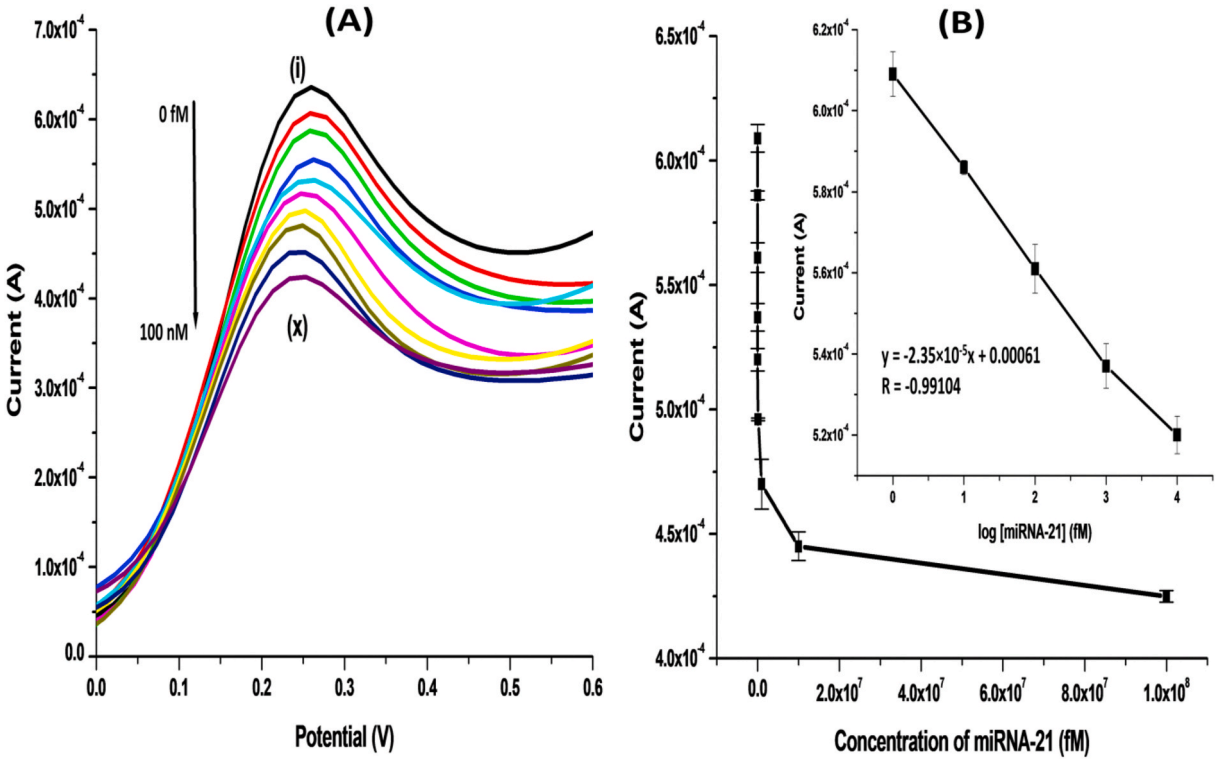

Fig. 4. (A) DPV response of bioelectrode after incubation with varying concentration of miRNA-21 (i.e. 0 fM, 1 fM, 10 fM, 100 fM, 1 pM, 10 pM, 100 pM, 1 nM, 10 nM and 100 nM), **(B)** Current response v/s miRNA-21 concentration from 1 fM to 1×10^9 fM (Inset: The linear relationship between current response and log of miRNA-21 concentration).

10^6 Hz. In the EIS spectrum, the diameter of a semicircle represents electron transfer resistance (R_{ct}) at the electrode surface whereas the linear part corresponds to the diffusion of the electrolyte solution. Thus, the results obtained from the EIS measurements must be negatively related to the CV and DPV results. The EIS results have been summarized depending on the R_{ct} values obtained. The Rct value for APTS/FTO was found to be 709 Ω which is higher than the R_{ct} value of AuPtBNPs/APTS/FTO (36.3 Ω) showing almost straight line due to the excellent electron transfer properties of AuPtBNPs. Further, the R_{ct} values increases to 77 Ω, 102 Ω and 361 Ω with stepwise fabrication of GA/AuPtBNPs/APTS/FTO, Am-cDNA/GA/AuPtBNPs/APTS/FTO and miRNA-21 coated Am-cDNA/GA/AuPtBNPs/APTS/FTO, respectively attributing to the blocking of electron transfer from electrolyte solution to the electrode surface.

Also the electrochemical analysis (CV and EIS) of mono as well as bimetallic nanoparticles coated APTS/FTO electrode has been shown in Fig. S1. The peak current of AuPtBNPs coated APTS/FTO electrode showed highest current (6.1×10^{-4} A) response in comparison to both the mono-metallic nanoparticles coated electrode i.e. 4.43×10^{-4} A and 4.82×10^{-4} A for Au/APTS/FTO and Pt/APTS/FTO, respectively. The EIS results are also supporting CV results, having R_{ct} values 88 Ω, 66 Ω and 56 Ω for the electrodes Au/APTS/FTO, Pt/APTS/FTO and AuPtBNPs/APTS/FTO, respectively. Hence, the results suggest effective use of AuPtBNPs/APTS/FTO electrode as a biosensing platform for miRNA-21 detection.

3.3.2. Electroactive surface area

The electroactive surface area of various modification done on FTO electrode surface was calculated using the Eq. $A = Ipa/2.69 \times 10^5 An^{3/2}C_oD_r^{1/2}\nu^{1/2}$. The CV measurements of all the electrodes were taken at varying scan rates from 10 mVs^{-1} to 100 mVs^{-1} in electrolyte solution (Fig. S2) and the slope obtained from the graph ($Ipa/\nu^{1/2}$) were used for carrying out further calculations. The equation can be re-written as

$$A = Ipa/2.69 \times 10^5\ An^{3/2}C_oD_r^{1/2}\ \nu^{1/2} \quad [1]$$

Where, A = surface area of the electrode (cm^2), I_{pa} = anodic peak current, n = number of electrons involved in the redox reaction (1), C_0 = concentration of $[Fe(CN)_6]^{3-/4-}$ (5 mol cm^{-3}), D_r = diffusion coefficient (7.6×10^{-6} cm^2 s^{-1}) and v = scan rate (Vs^{-1}). The effective surface area of APTS/FTO, AuPtBNPs/APTS/FTO, GA/AuPtBNPs/APTS/FTO and Am-cDNA/GA/AuPtBNPs/APTS/FTO was found to be 0.163 cm^2, 0.3244 cm^2, 0.2973 cm^2 and 0.2432 cm^2, respectively. Because of the highly conductive nature of AuPtBNPs, the matrix used for the development of biosensor (i.e. AuPtBNPs/APTS/FTO) has shown considerable increase in the electroactive surface area.

3.4. Optimization of study parameters

The amount of Am-cDNA probe and hybridization time required for the significant detection of miRNA-21 was optimized by using DPV responses. The glutaraldehyde coated AuPtBNPs/APTS/FTO electrode surface was treated with a range of cDNA probe concentrations i.e. 0 μM, 1 μM, 5 μM, 10 μM, 15 μM, 20 μM and 25 μM. The electrodes were stored at 4 °C until drying and current responses were measured after washing the unbound particles. As shown in Fig. S3 (A), the bioelectrodes displayed decreased current response with increasing concentration up to 20 μM of cDNA probe concentration. This might be due to the fact that binding sites present on the surface of GA/AuPtBNPs/APTS/FTO electrode for cDNA probe gets saturated and no further decrease in the current response was observed after 20 μM. Hence, 20 μM was selected as optimized concentration.

The hybridization time required for the formation of duplex structure between cDNA probe and miRNA-21 was also examined. Fig. S3 (B) shows the effect of different time intervals (i.e. 0,5,10,15,20,25 and 30 min) on the current response of bioelectrode. As the hybridization time increased, the current response decreased and reached to a plateau after 20 min. Due to the complete binding of active sites present on electrode surface, 20 min was chosen as suitable hybridization time for carrying

Table 1
Comparison of present biosensor with other miRNA-21 based biosensors.

Signal amplification approach	Analytical method of detection	Linear range	Detection limit	Response time	References
Duplex-specific nuclease assisted target recycling	EIS	0.5–40 fM	60 aM	30 min	[30]
Strand displacement reaction amplification strategy	Amperometry/I-T measurements	1 fM- 1 nM	0.34 fM	90 min	[31]
Single enzyme amplification and electrochemical–chemical–chemical redox cycling	Amperometry	0.5 fM-1 pM	0.2 fM	60 min	[32]
Catalytic hairpin assembly and rolling circle amplification as a dual signal amplification strategy	DPV	0.5–12500 pM	290 fM	90 min	[33]
Au nanorods modified microfluidic paper-based analytical devices	DPV	1-1000 fM	0.434 fM	2 h	[34]
DNA hybridization chain reaction	Fluorescence assay	1-10^5 fM	0.2554 fM	2 h	[35]
Molecular beacon mediated strand displacement amplification and enzymatic amplification	DPV	10–50 pM	40 pM	90 min	[36]
Electrochemical–chemical–chemical redox cycling	DPV	0.1 fM-0.1 pM	0.086 fM	60 min	[37]
Catalytic hairpin assembly	DPV	1 fM-1 nM	0.33 fM	100 min	[38]
Duplex-specific nuclease-assisted target recycling	Amperometry	0.1 fM-100 pM	43.3 aM	50 min	[39]
Voltammetric hybridization assay	DPV	1 fM-1 μM	1 fM	20 min	[40]
Voltammetric hybridization assay	DPV	1 fM-100 nM	0.63 fM	20 min	This work

out further experiments.

3.5. Detection of miRNA-21

The performance of developed biosensor was tested for different concentrations of miRNA-21 using DPV technique under optimum experimental conditions. It can be seen from Fig. 4A, that the current response of Am-cDNA/GA/AuPtBNPs/APTS bioelectrode tends to decrease linearly with increasing miRNA-21 concentration from 1 fM-100 nM. This decrease might be attributed to the amount of duplex formed after hybridization with miRNA-21. As the concentration of miRNA-21 increased, the negatively charged phosphate moieties also increased with duplex formation and the transfer of electrons becomes difficult from the ferri-ferro electrolyte solution. The bioelectrode incubated with 1 fM of miRNA-21 concentration exhibited very close current response to the bare electrode whereas 100 nM of miRNA-21 concentration shows lowest current response. Further, the limit of detection 0.63 fM was calculated from the formula

$$LOD = 3SD/m \quad [2]$$

(where, SD = standard deviation of electrode without any target and m = slope of the calibration plot).

The change in the current response with increasing miRNA-21 concentration from 1 fM to 1 × 10^9 fM was plotted in Fig. 4B. However, a calibration plot is also given in the inset Fig, between the log of miRNA-21 concentrations v/s current responses. The slope obtained from inset graph was used to calculate LOD of presented biosensor, showing a regression equation

$$y = -2.35 \times 10^{-5}x + 6.107 \times 10^{-4} \quad [3]$$

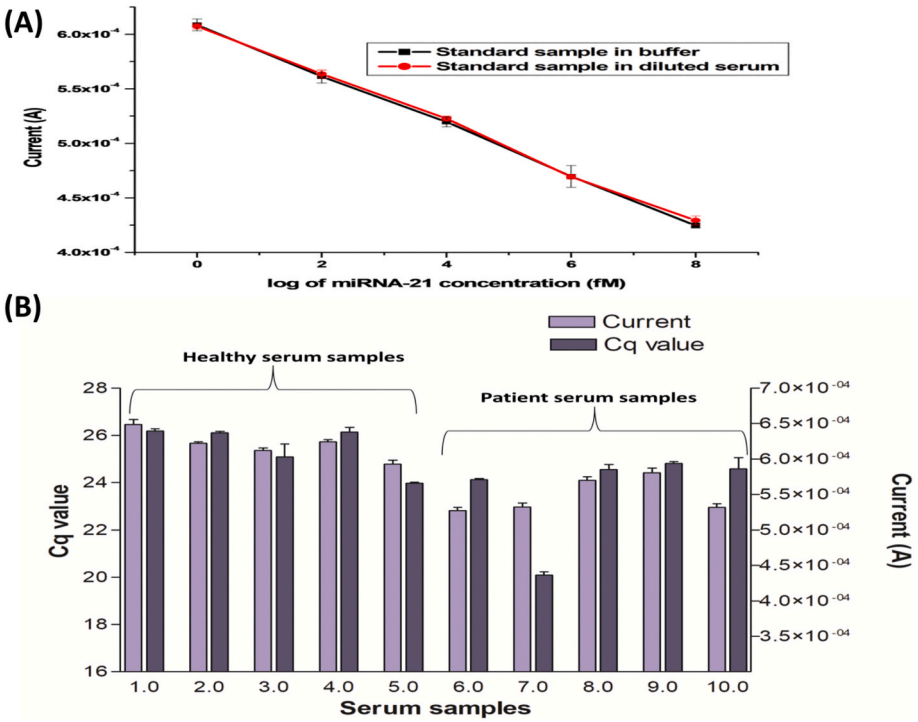

Fig. 5. (A) Current response of selected miRNA-21 concentrations (i.e. 1 fM, 1 × 10^2 fM, 1 × 10^4 fM, 1 × 10^6 fM and 1 × 10^8 fM) prepared in buffer (black) and diluted serum (red), **(B)** Real time-PCR expression levels and current responses of healthy (1–5) and patient (6–10) serum samples for miRNA-21 detection. (For interpretation of the references to color in this figure legend, the reader is referred to the Web version of this article.)

Table 2
Recovery percentage of spiked serum samples (n = 3).

S.No.	Added (nM)	Found (nM)	Recovery %	RSD
1	0.001	0.000901	90.18	4.82%
2	0.1	0.0921	92.1	1.80%
3	1	0.946	94.6	2.59%
4	10	9.38	93.6	6.33%

(where, y = current response and x = log of miRNA-21 concentration in fM).

Correlation coefficient = −0.99104.

Table 1 summarizes the signal amplification approach, analytical method of detection, linear ranges and detection limits of other previously described strategies and compares them with present biosensing strategy. The biosensor exhibits very high sensitivity and good linear range of detection approaching other biosensing strategies, with better response time among all. But many lengthy and complicated steps of immobilization and modifications have been excluded in the present work, proving it a very quick, easy and cost effective method for miRNA-21 detection. The satisfying results can be attributed to the number of advantages associated with the biosensing platform such as high conductivity, physical stability and binding affinity.

3.6. Real sample studies

To check the feasibility of development biosensor, different concentrations of miRNA-21 within a range from 1 fM to 100 nM were prepared using 10 fold diluted serum and applied for electrochemical detection. The miRNA-21 concentrations prepared in diluted serum shows very similar trend in their current response as obtained from the miRNA-21 concentrations prepared in buffer (Fig. 5A). Hence, it can be concluded that the developed biosensor is sensitive enough and could be used for real sample analysis. The recovery percentage of spiked samples was also calculated using the formula

$$\text{Found concentration} = (\text{Test current/standard current}) \times \text{standard concentration} \quad [4]$$

$$\text{Recovery \%} = (\text{found concentration/spiked concentration}) \times 100 \quad [5]$$

Recovery percentage ranging from 90.18% to 94.6% was obtained in spiked serum samples with RSD ranging from 1.80% to 6.33% as shown in Table 2. Hence, the bioelectrode could be efficiently applied in the clinical analysis of miRNA-21 detection.

3.7. Electrochemical vs. real time-PCR analysis

The current response and real time-PCR expression for both the healthy and patient serum samples are shown in Fig. 5B. It was found

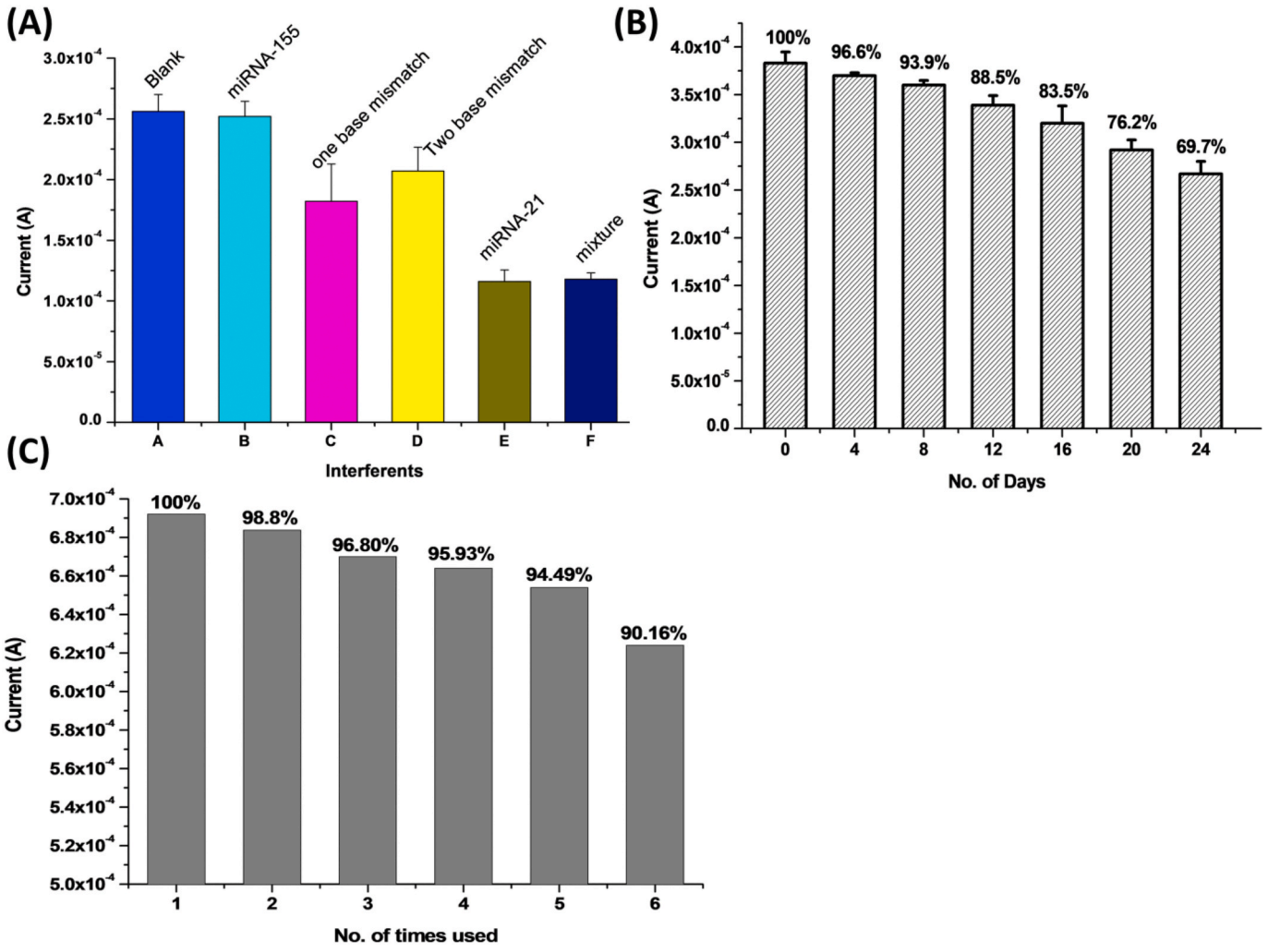

Fig. 6. (A) Histogram obtained after incubating the bioelectrode with various interferent molecules, **(B)** Storage stability of the bioelectrode up to 24 days at an interval of four days, and **(C)** Regeneration of the bioelectrode after treatment with miRNA-21 up to 6 times.

that the higher peak current in normal samples shows lower level of miRNA-21 whereas the peak current decreased in case of patient samples indicated the presence of significant amount of miRNA-21. Similarly, the C_q values of healthy samples were higher than the C_q values of patient samples due to the presence of greater amount of miRNA-21 in breast cancer patients. The value of correlation coefficient was found to be 0.708, suggesting that the results obtained from presented electrochemical method are strongly related with the real time-PCR results.

3.8. Selectivity and stability of developed biosensor

The ability to distinguish between the target probe and mutated targets like one base mismatch, two base mismatch & non-target probe is a significant approach to test the performance of developed biosensor. In Fig. 6A, a comparative study was evaluated by measuring the current response of Am-cDNA/GA/AuPtBNPs/APTS/FTO electrode coated with, miRNA-21, one base mismatch target, two base mismatch target, miRNA-155 and mixture of all the samples at a concentration of 1 μM each. The current response significantly decreased in case of miRNA-21 and mixture solution; whereas non–target probe bound electrodes showed nearly same response to the blank electrode. This might be due to the unbinding of these non-target sequences after washing which does not hybridized effectively with the developed bioelectrode. Moreover, to further improve the applicability of designed biosensor, the storage stability was also determined. As prepared Am-cDNA/GA/AuPtBNPs/APTS/FTO electrode was stored at 4 °C and used for the detection of miRNA-21 (100 nM) every fourth day up to 24 days. Fig. 6B shows the change in DPV response after every 4 day and bioelectrode shows 88% of its original current value after 12 days. Hence, the bioelectrode is found to be selective enough for its target miRNA and is stable for 12 days.

3.9. Reproducibility and reusability of developed biosensor

Reproducibility is an important parameter to test the reliability of synthesized biosensor. For this study, three independent bioelectrodes were subjected for the detection of 1 pM miRNA-21 on same day and other three on next subsequent days. Similarly, the bioelectrode was also applied for other two miRNA-21 concentrations i.e. 10 pM and 1 nM. It can be seen from Fig. S4 that all the bioelectrodes incubated with same amount of miRNA-21 showed constant current response. The relative standard deviation is 1.76% and 2.23% for 1 pM, 3.75% and 3.56% for 10 pM and 3.48% and 4.45% for 1 nM on same day and different days, respectively.

The bioelectrode was also reused after regeneration with 50 mM of NaOH solution for 10 min. After washing with dH_2O, the electrode was further used for miRNA-21 detection. As shown in Fig. 6C, the electrode exhibited current response 100%, 98.8%, 96.80%, 95.93%, 94.49% and 90.16% after regenerating it for 6 times. So, the results suggested that the bioelectrode is highly reproducible andreusable upto 6 time with retaining 90.16 % of initial current value.

4. Conclusions

An electrochemical biosensor was successfully employed for hybridization based detection of miRNA-21 using aminylated cDNA as biorecognition element. The biosensing platform utilized APTS as well as AuPtBNPs as matrix material to immobilize cDNA probe on the electrode surface through glutaraldehyde linker. Under optimized experimental conditions the biosensor showed limit of detection up to 0.63 fM and linear range of detection 1 fM-100 nM for miRNA-21. The biosensor also exhibit high specificity for its target, stability of 12 days, reusability of about 6 times withappreciable reproducibility. The spike-in studies done using diluted serum samples have also shown good recovery range, suggesting its potential applicability in clinically relevant assays.

Author's contribution

Anu Bharti: Conceptualization, Methodology, Data curation, Writing- original draft preparation.

Sakshi Mittal: Investigation, Visualization.

Shilpa Rana: Visualization.

Divya Dahiya: Resources.

Nirmal Prabhakar: Writing- review & editing, Supervision, Project administration.

Navneet Agnihotri: Review and editing, Supervision, Project administration.

Acknowledgements

We highly acknowledge the financial support obtained from Special Assistance Programme (UGC-SAP) [F.4–7/2015/DRS-III (SAP-II)], DST-Purse II and DST-SERB [EEQ/2017/000239]. University sophisticated analytical instrumentation facility (SAIF) is also acknowledged for FE-SEM studies. I also want to thank CSIR for providing the award of fellowship [09/135(0729)/2016-EMR-I].

Appendix A. Supplementary data

Supplementary data to this article can be found online at https://doi.org/10.1016/j.ab.2020.113908.

References

[1] Y.S. Lee, A. Dutta, MicroRNAs in cancer, Annu. Rev. Pathol. 4 (2009) 199–227.
[2] B. Zhao, Q. Yu, H. Li, X. Guo, X. He, Characterization of microRNA expression profiles in patients with intervertebral disc degeneration, Int. J. Mol. Med. 33 (1) (2014) 43–50.
[3] W. Tan, B. Liu, S. Qu, G. Liang, W. Luo, C. Gong, MicroRNAs and cancer: key paradigms in molecular therapy, Oncol. Lett. 15 (3) (2018) 2735–2742.
[4] S. Juzenas, G. Venkatesh, M. Hubenthal, M.P. Hoeppner, Z.G. Du, M. Paulsen, P. Rosenstiel, P. Senger, M. Hofmann-Apitius, A. Keller, L. Kupcinskas, A. Franke, G. Hemmrich-Stanisak, A comprehensive, cell specific microRNA catalogue of human peripheral blood, Nucleic Acids Res. 45 (16) (2017) 9290–9301.
[5] A. Kozomara, M. Birgaoanu, S. Griffiths-Jones, miRBase: from microRNA sequences to function, Nucleic Acids Res. 47 (D1) (2019) D155–D162.
[6] Y. Peng, C.M. Croce, The role of MicroRNAs in human cancer, Signal Transduct. Targeted Ther. 1 (2016) 15004.
[7] T. Matsumura, K. Sugimachi, H. Iinuma, Y. Takahashi, J. Kurashige, G. Sawada, M. Ueda, R. Uchi, H. Ueo, Y. Takano, Y. Shinden, H. Eguchi, H. Yamamoto, Y. Doki, M. Mori, T. Ochiya, K. Mimori, Exosomal microRNA in serum is a novel biomarker of recurrence in human colorectal cancer, Br. J. Canc. 113 (2) (2015) 275–281.
[8] Y. Lin, F. Chen, L. Shen, X. Tang, C. Du, Z. Sun, H. Ding, J. Chen, B. Shen, Biomarker microRNAs for prostate cancer metastasis: screened with a network vulnerability analysis model, J. Transl. Med. 16 (1) (2018) 134.
[9] R. Hamam, D. Hamam, K.A. Alsaleh, M. Kassem, W. Zaher, M. Alfayez, A. Aldahmash, N.M. Alajez, Circulating microRNAs in breast cancer: novel diagnostic and prognostic biomarkers, Cell Death Dis. 8 (2017) e3045.
[10] X. Liu, Y. Qin, C. Deng, J. Xiang, Y. Li, A simple and sensitive impedimetric aptasensor for the detection of tumor markers based on gold nanoparticles signal amplification, Talanta 132 (2015) 150–154.
[11] A. Yokoi, J. Matsuzaki, Y. Yamamoto, Y. Yoneoka, K. Takahashi, H. Shimizu, T. Uehara, M. Ishikawa, S.I. Ikeda, T. Sonoda, J. Kawauchi, S. Takizawa, Y. Aoki, S. Niida, H. Sakamoto, K. Kato, T. Kato, T. Ochiya, Integrated extracellular microRNA profiling for ovarian cancer screening, Nat. Commun. 9 (1) (2018) 4319.
[12] M. Akram, M. Iqbal, M. Daniyal, A.U. Khan, Awareness and current knowledge of breast cancer, Biol. Res. 50 (1) (2017) 33.
[13] L.X. Yan, Q.N. Wu, Y. Zhang, Y.Y. Li, D.Z. Liao, J.H. Hou, J. Fu, M.S. Zeng, J.P. Yun, Q.L. Wu, Y.X. Zeng, J.Y. Shao, Knockdown of miR-21 in human breast cancer cell lines inhibits proliferation, in vitro migration and in vivo tumor growth, Breast Cancer Res. 13 (1) (2011) R2.
[14] S. Gao, H. Tian, Y. Guo, Y. Li, Z. Guo, X. Zhu, X. Chen, miRNA oligonucleotide and sponge for miRNA-21 inhibition mediated by PEI-PLL in breast cancer therapy, Acta Biomater. 25 (2015) 184–193.
[15] B. Savari, S. Boozarpour, M. Tahmasebi-Birgani, H. Sabouri, S.M. Hosseini, Overexpression of microRNA-21 in the serum of breast cancer patients, Microrna 9 (2020) 58–63.
[16] K.A. Hug, L. Anthony, D. Eldeiry, J. Benson, E. Wheeler, S. Mousa, B. Shi, Expression and tissue distribution of MicroRNA-21 in malignant and benign breast Tissues>, Anticancer Res. 35 (6) (2015) 3175–3183.
[17] G.A. Calin, C.M. Croce, MicroRNA signatures in human cancers, Nat. Rev. Canc. 6 (11) (2006) 857–866.

[18] G.S. Pall, C. Codony-Servat, J. Byrne, L. Ritchie, A. Hamilton, Carbodiimide-mediated cross-linking of RNA to nylon membranes improves the detection of siRNA, miRNA and piRNA by northern blot, Nucleic Acids Res. 35 (8) (2007) e60.
[19] E. Clancy, M. Burke, V. Arabkari, T. Barry, H. Kelly, R.M. Dwyer, M.J. Kerin, T. J. Smith, Amplification-free detection of microRNAs via a rapid microarray-based sandwich assay, Anal. Bioanal. Chem. 409 (14) (2017) 3497–3505.
[20] C.F. Chen, D.A. Ridzon, A.J. Broomer, Z.H. Zhou, D.H. Lee, J.T. Nguyen, M. Barbisin, N.L. Xu, V.R. Mahuvakar, M.R. Andersen, K.Q. Lao, K.J. Livak, K. J. Guegler, Real-time quantification of microRNAs by stem-loop RT-PCR, Nucleic Acids Res. 33 (20) (2005) e179.
[21] H. Zhang, M. Fan, J. Jiang, Q. Shen, C. Cai, J. Shen, Sensitive electrochemical biosensor for MicroRNAs based on duplex-specific nuclease-assisted target recycling followed with gold nanoparticles and enzymatic signal amplification, Anal. Chim. Acta 1064 (2019) 33–39.
[22] L. Yang, C. Liu, W. Ren, Z. Li, Graphene surface-anchored fluorescence sensor for sensitive detection of microRNA coupled with enzyme-free signal amplification of hybridization chain reaction, ACS Appl. Mater. Interfaces 4 (12) (2012) 6450–6453.
[23] H. Vaisocherova, H. Sipova, I. Visova, M. Bockova, T. Springer, M.L. Ermini, X. Song, Z. Krejcik, L. Chrastinova, O. Pastva, K. Pimkova, M. Dostalova Merkerova, J.E. Dyr, J. Homola, Rapid and sensitive detection of multiple microRNAs in cell lysate by low-fouling surface plasmon resonance biosensor, Biosens. Bioelectron. 70 (2015) 226–231.
[24] J. Zhuang, W. Lai, G. Chen, D. Tang, A rolling circle amplification-based DNA machine for miRNA screening coupling catalytic hairpin assembly with DNAzyme formation, Chem. Commun. (Camb.) 50 (22) (2014) 2935–2938.
[25] B. Cai, L. Huang, H. Zhang, Z. Sun, Z. Zhang, G.J. Zhang, Gold nanoparticles-decorated graphene field-effect transistor biosensor for femtomolar MicroRNA detection, Biosens. Bioelectron. 74 (2015) 329–334.
[26] W.C. Zhang, J.Q. Zhang, Q. Zhang, F. Hu, W.J. Han, Y.Q. Gu, Highly specific real-time qualification of diverse microRNAs in tissue and serum using universal molecular beacon, Sensor. Actuator. B Chem. 262 (2018) 153–161.
[27] J. Liu, H. Zhou, J.J. Xu, H.Y. Chen, An effective DNA-based electrochemical switch for reagentless detection of living cells, Chem. Commun. (Camb.) 47 (15) (2011) 4388–4390.
[28] A. Jamil, H.N. Lim, N.A. Yusof, A.A. Tajudin, N.M. Huang, A. Pandikumar, A. M. Golsheikh, Y.H. Lee, Y. Andou, Preparation and characterization of silver nanoparticles-reduced graphene oxide on ITO for immunosensing platform, Sensor. Actuator. B Chem. 221 (2015) 1423–1432.
[29] M. Cui, Y. Wang, H.P. Wang, Y.M. Wu, X.L. Luo, A label-free electrochemical DNA biosensor for breast cancer marker BRCA1 based on self-assembled antifouling peptide monolayer, Sensor. Actuator. B Chem. 244 (2017) 742–749.
[30] J. Zhang, D.Z. Wu, S.X. Cai, M. Chen, Y.K. Xia, F. Wu, J.H. Chen, An immobilization-free electrochemical impedance biosensor based on duplex-specific nuclease assisted target recycling for amplified detection of microRNA, Biosens. Bioelectron. 75 (2016) 452–457.
[31] L. Tian, J. Qi, X. Ma, X. Wang, C. Yao, W. Song, Y. Wang, A facile DNA strand displacement reaction sensing strategy of electrochemical biosensor based on N-carboxymethyl chitosan/molybdenum carbide nanocomposite for microRNA-21 detection, Biosens. Bioelectron. 122 (2018) 43–50.
[32] N. Xia, Y. Zhang, X. Wei, Y. Huang, L. Liu, An electrochemical microRNAs biosensor with the signal amplification of alkaline phosphatase and electrochemical-chemical-chemical redox cycling, Anal. Chim. Acta 878 (2015) 95–101.
[33] Q. Li, F. Zeng, N. Lyu, J. Liang, Highly sensitive and specific electrochemical biosensor for microRNA-21 detection by coupling catalytic hairpin assembly with rolling circle amplification, Analyst 143 (10) (2018) 2304–2309.
[34] X. Sun, H. Wang, Y. Jian, F. Lan, L. Zhang, H. Liu, S. Ge, J. Yu, Ultrasensitive microfluidic paper-based electrochemical/visual biosensor based on spherical-like cerium dioxide catalyst for miR-21 detection, Biosens. Bioelectron. 105 (2018) 218–225.
[35] Z. Li, B. Li, Y. Zhou, H. Yin, J. Wang, S. Ai, Ultrasensitive microRNA-21 detection based on DNA hybridization chain reaction and SYBR Green dye, Anal. Biochem. 538 (2017) 20–25.
[36] M.N. Wang, B. Shen, R. Yuan, W. Cheng, H.B. Xu, S.J. Ding, An electrochemical biosensor for highly sensitive determination of microRNA based on enzymatic and molecular beacon mediated strand displacement amplification, J. Electroanal. Chem. 756 (2015) 147–152.
[37] H.L. Shuai, K.J. Huang, Y.X. Chen, L.X. Fang, M.P. Jia, Au nanoparticles/hollow molybdenum disulfide microcubes based biosensor for microRNA-21 detection coupled with duplex-specific nuclease and enzyme signal amplification, Biosens. Bioelectron. 89 (2017) 989–997.
[38] S.H. Liu, Z.H. Yang, Y.Y. Chang, Y.Q. Chai, R. Yuan, An enzyme-free electrochemical biosensor combining target recycling with Fe_3O_4/CeO_2@Au nanocatalysts for microRNA-21 detection, Biosens. Bioelectron. 119 (2018) 170–175.
[39] H. Zhang, M.X. Fan, J.Q. Jiang, Q.M. Shen, C.X. Cai, J. Shen, Sensitive electrochemical biosensor for MicroRNAs based on duplex-specific nuclease-assisted target recycling followed with gold nanoparticles and enzymatic signal amplification, Anal. Chim. Acta 1064 (2019) 33–39.
[40] A. Bharti, N. Agnihotri, N. Prabhakar, A voltammetric hybridization assay for microRNA-21 using carboxylated graphene oxide decorated with gold-platinum bimetallic nanoparticles, Microchim Acta 186 (3) (2019).
[41] M. Cui, J.D. Huang, Y. Wang, Y.M. Wu, X.L. Luo, Molecularly imprinted electrochemical sensor for propyl gallate based on PtAu bimetallic nanoparticles modified graphene-carbon nanotube composites, Biosens. Bioelectron. 68 (2015) 563–569.
[42] M.D. Li, P. Wang, F.Y. Li, Q.Y. Chu, Y.Y. Li, Y.H. Dong, An ultrasensitive sandwich-type electrochemical immunosensor based on the signal amplification strategy of mesoporous core-shell Pd@Pt nanoparticles/amino group functionalized graphene nanocomposite, Biosens. Bioelectron. 87 (2017) 752–759.
[43] M.M. Eteya, G.H. Rounaghi, B. Deiminiat, Fabrication of a new electrochemical sensor based on Au-Pt bimetallic nanoparticles decorated multi-walled carbon nanotubes for determination of diclofenac, Microchem. J. 144 (2019) 254–260.
[44] U. Jain, S. Gupta, N. Chauhan, Construction of an amperometric glycated hemoglobin biosensor based on Au-Pt bimetallic nanoparticles and poly (indole-5-carboxylic acid) modified Au electrode, Int. J. Biol. Macromol. 105 (2017) 549–555.
[45] S. Shahrokhian, S. Rastgar, Construction of an electrochemical sensor based on the electrodeposition of Au-Pt nanoparticles mixtures on multi-walled carbon nanotubes film for voltammetric determination of cefotaxime, Analyst 137 (11) (2012) 2706–2715.
[46] E. Zor, I.H. Patir, H. Bingol, M. Ersoz, An electrochemical biosensor based on human serum albumin/graphene oxide/3-aminopropyltriethoxysilane modified ITO electrode for the enantioselective discrimination of D- and L-tryptophan, Biosens. Bioelectron. 42 (2013) 321–325.
[47] D. Zheng, S.K. Vashist, K. Al-Rubeaan, J.H.T. Luong, F.S. Sheu, Rapid and simple preparation of a reagentless glucose electrochemical biosensor, Analyst 137 (16) (2012) 3800–3805.
[48] S.Y. Li, W.H. Ma, Y. Zhou, X.H. Chen, M.Y. Ma, Y.H. Xu, Z. Ding, X.H. Wu, 3-aminopropyltriethoxysilanes modified porous silicon as a voltammetric sensor for determination of silver ion, Int. J. Electrochem. Sci. 8 (2) (2013) 1802–1812.
[49] K.S. Aneja, S. Bohm, A.S. Khanna, H.L.M. Bohm, Graphene based anticorrosive coatings for Cr(VI) replacement, Nanoscale 7 (42) (2015) 17879–17888.
[50] H.S. Mansur, C.M. Sadahira, A.N. Souza, A.A.P. Mansur, FTIR spectroscopy characterization of poly (vinyl alcohol) hydrogel with different hydrolysis degree and chemically crosslinked with glutaraldehyde, Mater. Sci. Eng. C Bio Sci. 28 (4) (2008) 539–548.
[51] A. Salimi, B. Kavosi, A. Navaee, Amine-functionalized graphene as an effective electrochemical platform toward easily miRNA hybridization detection, Measurement 143 (2019) 191–198.
[52] K. Arora, N. Prabhakar, S. Chand, B.D. Malhotra, Ultrasensitive DNA hybridization biosensor based on polyaniline, Biosens. Bioelectron. 23 (5) (2007) 613–620.